ADVANCED THEORY AND SIMULATIONS
www.advtheorysimul.com

# On the Crack-Tip Region Stress Field in Molecular Systems: The Case of Ideal Brittle Fracture

*Pasquale Gallo*

**Continuum-based fracture mechanics breaks down at the nanoscale where the discrete nature of atoms cannot be neglected. Intriguingly, this work shows that the concept of stress intensity factor is still valid if the atoms are modeled. Molecular statistics simulations are conducted on single-edge cracked samples of ideal brittle silicon, varying the size until few nanometers. The local virial stress, derived as the functional derivative of the free energy of a molecular system with respect to the deformation tensor, is used as a measure of the mechanical stress at the atomic level. Then, stress intensity factor at failure is evaluated. The results show that regardless of the size, the atomistic stress field varies according to the classical $1/r^{0.5}$ relation, and discrete stress intensity factors can be derived for all the geometries. Continuum values, in contrast, fail to describe the fracture when the length of the singular stress field is smaller than 4–5 times the fracture process zone. Thus, this work shows that the stress intensity factor from atomic stress may be useful to describe the fracture criterion at extremely small dimensions, provided that virial stress is accepted as a representation of mechanical stress at the atomic level.**

## 1. Introduction

With recent developments in the field of nanotechnology, the size of components has been approaching a few nanometers. A classic example is provided by nano-electro-mechanical systems which have high-density integration and are commonly used as sensors and actuators, and flexible nanoelectronics.[1,2] These devices may have complex geometries and features such as notches and cracks, which are classic design issues addressed by linear elastic fracture mechanics (LEFM). However, at such a small scale, critical questions arise on the validity of the LEFM since continuum assumptions can be questioned. Therefore, several researchers have tried in the recent past to propose new approaches, extend classic ones, and to quantify the low limit of continuum-based fracture mechanics.[3–10] Studies are particularly numerous for ideal brittle fracture where atomistically informed fracture criteria are desirable, but works on other advanced materials are available as well.[11,12] Indeed, it is well-known that brittle fracture is ultimately governed by atomic bonds breaking.[13,14] Pugno et al.[15,16] proposed an energy-based theory, namely Quantized Fracture Mechanics, which modifies continuum-based fracture mechanics by introducing finite differences in Griffith's criterion.[17] Shimada et al.[18] quantified the breakdown of continuum fracture mechanics, that is, when the singular stress field at the crack-tip is in the range of 3–6 times the fracture process zone, and proposed a discrete-based energy release rate that goes beyond that limit. Similarly, extensions or reformulations of Griffith's criterion to take into account the discrete nature of atoms at extremely small scales have been also proposed by other researchers.[19,20] Alternatively, a reformulated strain energy density averaged over the fracture process zone has been successfully used to quantify the breakdown of continuum fracture mechanics and to characterize the fracture until a sample of few nanometers in length.[21] When the fracture mechanisms are more complex than the ones of ideal brittle fracture, simple approaches inspired by Griffith's energy balance may not be sufficient, and the fracture becomes a multiscale problem where transmission of the properties across scales is crucial.[22]–[26]

While energy-based approaches seem to be very successful in characterizing fracture at small scales, stress-based methods face additional challenges. Stress is indeed a continuum concept, and discussion on the difference between continuum stress and atomic stress is very delicate and challenging. Moreover, in the presence of defects, the classic formulation of Irwin (or Westergaard)[27,28] gives an "unrealistic" infinite stress at the crack-tip, in clear contradiction with atomistic simulations. When investigating fracture at the atomic scale by atomistic simulations, the stresses are usually extracted from the virial stress tensor, which is a measure of mechanical stress on the atomic scale. For homogenous systems, at zero Kelvin (i.e., all velocities are zero), the instantaneous volume averaged virial stress is given by

$$\sigma_{ij} = \frac{1}{2\Omega} \sum_{p,q \in \Omega} \left( x_i^{(q)} - x_i^{(p)} \right) f_j^{(pq)} \tag{1}$$

where $p$ and $q$ are indices of atoms inside the unit cell, $i$, $j$, are Cartesian indices, $\Omega$ is the volume, $x^{(q)}$ and $x^{(p)}$ are the positions

Dr. P. Gallo
Department of Mechanical Engineering
School of Engineering, Aalto University
P.O. Box 14100, FIN-00076 Aalto, Finland
E-mail: pasquale.gallo@aalto.fi

The ORCID identification number(s) for the author(s) of this article can be found under https://doi.org/10.1002/adts.201900146

**DOI: 10.1002/adts.201900146**

 

of the atoms $q$ and $p$. $f_j^{(pq)}$ is the $j$th component of the force between the atoms $p$ and $q$ computed by using interatomic potentials. There have been several studies investigating the near-tip stress distribution by use of the virial stress definition as well as trying to provide a sort of equivalence with the continuum stress.[29–33] Other works even questioned the validity of the virial stress as a representation of mechanical stress.[34] However, the studies available do not provide details on the evaluation of concepts like stress intensity factors and comparison with continuum solutions. In the present work, by considering the virial stress, the author demonstrates the existence of the trend of inverse square root singularity in the atomistic system for ideal brittle fracture and shows that computation of a stress intensity factor according to the classic Irwin's definition is possible. Moreover, through the comparison with the continuum finite-element (FE) method solutions, we defined a critical size at which continuum-based LEFM seems to fail. In contrast to previous works which focus on energy approaches as briefly summarized earlier, this paper evaluates, the breakdown of continuum-based LEFM by considering the stress analyses. The well-known modified Stillinger–Weber (SW) potential,[35] widely used to investigate stress concentration phenomena of silicon,[36] is employed. It is thus shown that the stress intensity factor from atomic stress may be beneficial to describe the fracture criterion at extremely small dimensions, provided that virial stress is accepted as a representation of mechanical stress at the atomic level.

It is worth noting that the equivalence between continuum and atomistic stress is not discussed and it is not the target of this study. Instead, focus lies on the stress distribution in the crack-tip region of a molecular system by considering the case of ideal brittle fracture. Continuum-based analyses are carried out only for a qualitative comparison and to evaluate the breakdown of continuum fracture mechanics. Therefore results are presented in a "normalized" form. The work is limited only to ideal brittle fracture, and single-edge cracked samples loaded under mode I.

## 2. Results: Crack-Tip Stress Field

The present work aims to investigate the crack-tip stress field from molecular statistics (MS) numerical experiments at failure conditions, and to compare the results with continuum-based FE analyses. To this aim, single-edge cracked samples depicted in **Figure 1** have been defined at several sizes. Specifically, the width $W$ has been varied from 198.41 nm down to 9.81 nm, while the crack length $a$ is kept equal to $W/3$. This choice ensures that regardless of effective crack length, condition of validity of continuum-based LEFM is always met, that is, small crack in an infinite plate. Finally, in order to ensure that there is no influence of the boundary conditions, the total height of the specimen is fixed to $2W$. **Table 1** summarizes the geometrical parameters of all the samples. The orientation of the specimens is also depicted in Figure 1: the crack plane coincides with the cleavage plane (111), and it is perpendicular to the direction [111]. Details of the MS numerical experiments and mechanical properties derived from the SW potential are reported in Section 5 and in ref. 21 where analyses in terms of strain energy density of similar samples is presented. A stepwise increment of strain ε is applied at the upper and lower layers of atoms of the specimens, as shown in Figure 1a, until the maximum critical displacement before final fracture, namely $d_C$, is reached. Therefore, critical displacement $d_C$ represents the failure condition, and values are summarized in Table 1. It should be noted that a linear behavior until final failure is observed for all samples, which are globally always under linear elastic conditions.[21] Moreover, phenomena such as atomic reconstruction, surface reconstruction, or phase transformation did not occur at the crack-tip or crack surfaces. Once the critical displacement is exceeded, the crack propagates instantaneously. The stress field of the geometries is investigated later by using FE analyses by applying the critical displacement $d_C$ obtained from the MS simulations (see Figure 1b and Section 5).

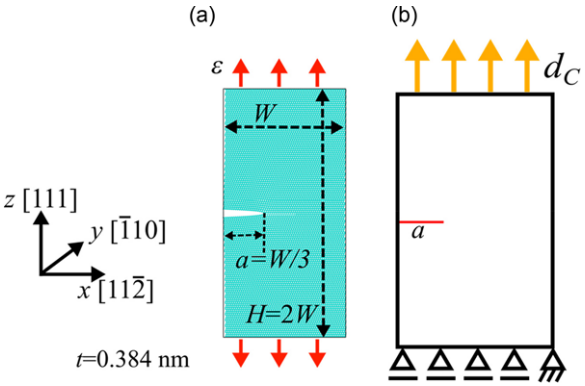


**Figure 1.** Schematics a) of the cracked samples and simulation box employed in the molecular statistics analyses (visualized through OVITO[52]), orientation, and b) constraints configuration of FE model with critical displacement; $t$ is the thickness of the simulation cell; the crack is slightly open to facilitate visualization.

**Table 1.** Specimens width $W$, displacement at fracture obtained from MS analyses $d_C$, and singular stress field lengths from continuum-based FE and MS analyses; the length is defined as the distance from crack-tip (or atom at crack-tip) at which the stresses deviate from the expected $1/r^{0.5}$ singularity; crack length $a = W/3$ while specimen height is $2W$.

| $W$ [nm] | $d_C$ [nm] | $\Lambda_K$ [a)] [nm] | $\Lambda_{K\text{-}MS}$ [b)] [nm] | $K_{If}$ [b)] [MPa$\sqrt{m}$] |
|---|---|---|---|---|
| 198.41 | 5.24 | 7.78 | ≈9.84 | 0.96 |
| 150.77 | 4.54 | 6.86 | ≈8.50 | 0.96 |
| 101.14 | 3.64 | 4.85 | ≈6.15 | 0.96 |
| 89.23 | 3.48 | 3.50 | ≈5.80 | 0.97 |
| 79.56 | 3.30 | 3.20 | ≈4.60 | 0.96 |
| 69.38 | 3.06 | 2.87 | ≈4.20 | 0.97 |
| 59.77 | 2.86 | 2.35 | ≈3.50 | 0.96 |
| 51.78 | 2.64 | 2.14 | ≈3.40 | 0.97 |
| 39.81 | 2.24 | 1.65 | ≈3.08 | 0.97 |
| 29.83 | 1.91 | 1.35 | ≈2.06 | 0.97 |
| 19.87 | 1.49 | 0.97 | ≈1.72 | 0.97 |
| 9.81 | 1.04 | 0.42 | ≈0.69–1.03 | 0.96 |

[a)] Obtained from continuum-based FE analyses; [b)] Obtained from MS analyses (atomic stress).

At the critical displacement $d_C$, the stress intensity factor at failure $K_{If}$ is evaluated according to the definition provided by

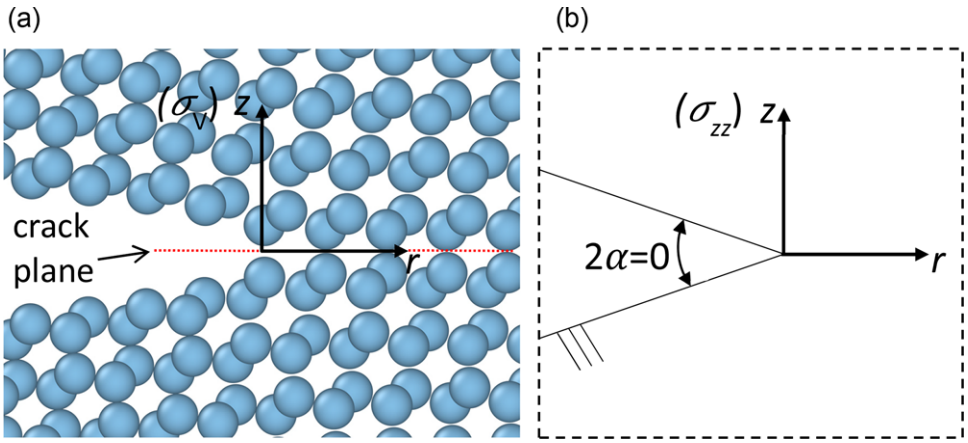


**Figure 2.** Close-up at crack-tip region of a) molecular system and b) continuum-based FE analyses.

Irwin.[27] In the case of the atomistic stress intensity factor it assumes the following form

$$K_{If} = \sigma_V \sqrt{2\pi r} \tag{2}$$

where $\sigma_V$ is the atomistic mechanical stress perpendicular to the crack plane from MS analyses according to the virial theorem, and $r$ is the distance from the crack-tip, along the crack plane. The crack is hypothetically centered between atoms at the crack-tip (see **Figure 2**a). It should be noted that atomic stress computed from MS analyses is a "stress × volume" formulation, meaning that the computed quantity is in units of "pressure × volume". Therefore, before employing MS atomic stress in Equation (2), it needs to be divided by a per-atom volume to have units of stress (pressure). In general, in simple configurations such as perfect crystal case, the per-atom volume is evaluated dividing the volume of the simulation cell by the number of atoms. However, this may be true when the simulation cell is filled by atoms entirely, that is, the system is homogenous, while it becomes questionable when the system is only partially occupied by atoms, for example in the case of crack or notch. In such configurations, the virial stress must be calculated by considering only the volume of the regions effectively filled by atoms. Besides, when the simulated system is subjected to relevant deformations, the volume should be re-evaluated at each strain level. Thus, each loading condition would have its own atomic volume. On top of these considerations, in the case of cracks or notches, some regions are severely deformed/stressed (e.g., crack-tip) while others are not. In this case, the volume may also change locally, meaning the virial stress should consider the local variation of volume. In the present work, the focus is on the stresses near the crack-tip in the critical condition (before final failure), in a region severely deformed and subjected to stress and strain very close to the ideal material strength (i.e., the strength of a component defect-free). For this reason, to obtain the correct stress state near the crack-tip, the atomic volume at high strain state (close to the critical strain of the ideal material strength) has been employed. The value is then kept constant for simplicity. The current SW potential gives an ideal material strength $\sigma_{IS}$ of 35.2 GPa in the direction [111], at a critical strain $\varepsilon_C$ of 0.3.[21] At these conditions, the per-atom volume is 24.55 Å$^3$, clearly larger than the volume generated by the lattice constant, that is, 20.01 Å$^3$. It seems this problem is generated by the fact that, in the case of cracks and notches, the assumption of homogeneity does not hold for the reasons explained above. This aspect is well-known and addressed by several other researchers[29,37]–[39] by imposing the convergence of local and whole volume-averaged virial stress of a perfect crystal.

On the other hand, the continuum-based stress intensity factor at failure is

$$K_{If} = \sigma_{zz} \sqrt{2\pi r} \tag{3}$$

where $\sigma_{zz}$ is the stress obtained from FE analyses perpendicular to the crack plane, and $r$ is the distance from the crack-tip along the crack plane (see Figure 2b).

**Figure 3** shows the crack-tip stress fields from MS analyses only for some selected geometries for the sake of clarity. It is worth recalling that the atomistic mechanical stress $\sigma_V$ in Figure 3 is effectively expressed as a pressure (per-atom volume already considered). Stress intensity factors at the critical displacement $d_C$ are depicted in **Figure 4**. These results are discussed in Section 3.

## 3. Discussion

At first look at Figure 3a, it is clear that the MS analyses do not predict infinite stress at crack-tip. The stress at the crack-tip is, indeed, almost identical to the ideal material strength $\sigma_{IS}$ of 35.2 GPa. These results indicate that the fracture is ultimately governed by the bond of atoms at the crack-tip. When the stress on these atoms reaches the ideal material strength, the crack propagates instantaneously by breaking of the subsequent atomic bond. This "crack-tip bond-dominated fracture" in the case of ideal brittle material is well-known and verified by several other authors who employed more sophisticated analyses, for example density functional theory calculations.[20] The missing singularity, instead, has been a long-standing concern in the scientific community, which led to questions on the validity of linear elasticity theory in the vicinity of the crack-tip region. Results in Figure 3b clearly show that even if the singularity is missing in the atomistic model, close to the crack-tip the stress still varies with

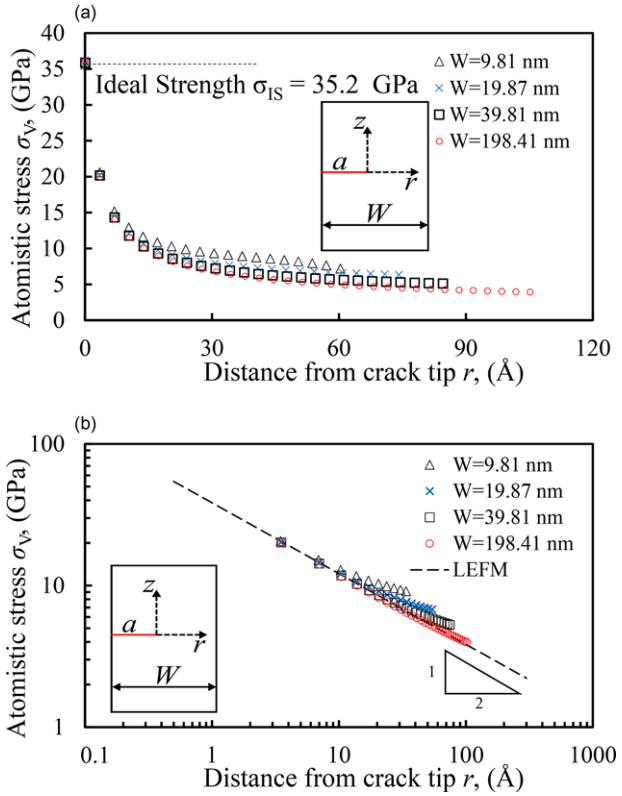


**Figure 3.** Crack-tip region stress fields from molecular statistics analyses based on virial theorem in a) linear and b) log–log scale; $\sigma_V$ is along the $z$ direction, perpendicular to the crack plane.

$1/r^{0.5}$ as expected from linear elastic theory. For the sake of clarity, Figure 3 reports only the results related to the specimen $W$ = 9.81, 19.87, 39.81, and 198.41 nm, respectively, but the trend is the same for all the considered geometries. When the sample scales down, the length of the inverse square root stress field also shrinks: the smallest sample $W = 9.81$ nm shows that variation with $1/r^{0.5}$ extends for ≈6.9–10.3 Å, therefore, for just a few atomic bonds from the crack-tip. The length increases to ≈98 Å for the largest specimen. This conclusion is relevant and further confirms what is found by other researchers[40]: the crack-tip region in a molecular system can be described by linear elastic fracture mechanics, at least in the case of static crack and ideal brittle material containing no other defects. Values of the length of $1/r^{0.5}$ stress fields are summarized in Table 1 and indicated as $\Lambda_{K\text{-}MS}$; the length of the singular stress fields from continuum-based FE analyses is reported as $\Lambda_K$. These values have been evaluated as the distance from atoms at the crack-tip at which the stress fields, $\sigma_V$ for MS analyses or $\sigma_{zz}$ for FE analyses, deviate more than 5% from the expected $1/r^{0.5}$ slope.

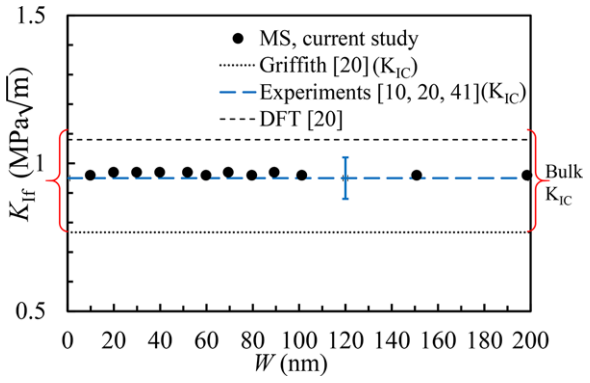


**Figure 4.** Stress intensity factor at failure $K_{If}$ from molecular statistics analyses versus the width of the samples $W$; the picture depicts also literature values of the "upper limit" of the fracture toughness from density functional theory (DFT), the "lower limit" given by Griffith's criterion, experimental values of small-scale silicon samples with scatter band, and bulk silicon specimens fracture toughness.

Based on these results, analyses on stress intensity factors at failure have been performed. Figure 4 depicts the stress intensity factor at failure $K_{If}$ versus the specimen width $W$ and the comparison with other works. The values have almost no variation, and all the samples seem to fail for the same $K_{If}$ of ≈0.97 MPa$\sqrt{m}$. Since $K_{If}$ is evaluated at fracture, it can be regarded as a good approximation of the fracture toughness, which shows a clear scale independence. The same picture demonstrates that values are in good agreement with experimental fracture toughness $K_{IC}$ of ≈ 0.95 ± 0.07 MPa$\sqrt{m}$ for micro, nano, and bulk silicon samples.[10,41] Also, it is within the range of expected "upper" and "lower" limit of $K_{IC}$, that is, 1.08 MPa$\sqrt{m}$ and 0.767 MPa$\sqrt{m}$, of which the first is evaluated by using density functional theory analyses including lattice trapping, while the second is the theoretical value provided by Griffith's criterion.[20,42] To investigate the behavior of the stress intensity factors at fracture on the continuum side, the values of $K_{If}$ are normalized with respect to the $K_{If}$ obtained for the largest specimen $W = 198.41$ nm and compared in **Figure 5**. It should be recalled that FE analyses are conducted based on the failure conditions obtained from MS analyses. As already mentioned in Section 1, the focus is on the trend of the $K_{If}$ rather than on a direct comparison of the stress fields between MS and continuum-based analyses which would require clarification on the equivalence between atomic and continuum stress. This is a challenging and complex topic that

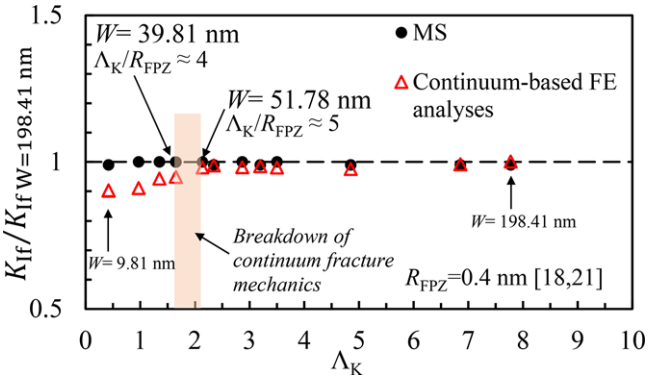


**Figure 5.** Normalized stress intensity factors at failure obtained from FE and MS analyses plotted against the length of the singular stress field, $\Lambda_K$, evaluated from continuum-based FE analyses; $\Lambda_K$ is defined as the distance from the crack-tip at which the stress deviates more than 5% from expected $1/r^{0.5}$ singularity; picture includes values of the fracture process zone $R_{FPZ}$ taken from the literature; from right to left, the points correspond to decreasing specimens width $W$, starting from $W$ = 198.41 nm (far-right point) to $W$ = 9.81 nm (far-left point); Table 1 reports numerical values.

deserves a specific paper. For the sake of clarity, it should be mentioned that the FE analyses give slightly larger stresses. A hypothesis is that employment, eventually, of two-parameters model[43] or inclusion of the T-stress[44] would correct the differences.[45] Going back to the results of Figure 5, the normalized $K_{If}$ are plotted against the length of the singular stress field *from FE analyses* $\Lambda_K$. For large specimens, a constant trend is obtained for both MS and continuum-based FE analyses. However, when the samples are reduced in size, the continuum-based normalized $K_{If}$ at failure starts to deviate from the expected ratio of 1. This result can be explained in terms of the breakdown of continuum-based fracture mechanics evaluated recently by other researchers.[18,21] The given references defined a so-called fracture process zone ($R_{FPZ}$) and *K*-dominant region $\Lambda_K$, that is, the length of the singular stress field showing the $1/r^{0.5}$ dependence (until a deviation of 5%, as in the present work). When reducing the sample width, the $R_{FPZ}$ remains constant, while the *K*-dominant region shrinks. If the $\Lambda_K$ remains geometrically larger than the fracture process zone, continuum-based fracture mechanics is valid; when the $\Lambda_K$ is geometrically approaching the $R_{FPZ}$, continuum-based fracture mechanics fails and shows an apparent size-dependent fracture toughness. In reality, this behavior is due to the fact that $\Lambda_K$ is not "large enough" in respect of the $R_{FPZ}$ as assumed by the continuum-based formulation, and it is not able to characterize the fracture. By assuming the $R_{FPZ}$ reported in the given references, that is 0.4 nm (average value), the continuum-based fracture mechanics fails for a critical $\Lambda_K/R_{FPZ}$ ratio of about 4–5. This result is in perfect agreement with values reported by other authors which evaluated similar range by using averaged strain energy density approach and energy release rate.[18,21] Therefore, provided that the virial stress is accepted as a representation of mechanical stress at the atomic level, the breakdown of the continuum-based fracture mechanics can also be evaluated in terms of stress from MS analyses. As a last comment on Figure 5, the same trend can be obtained if the normalized critical $K_{If}$ is plotted against specimen widths. Indeed, the *K*-dominant region $\Lambda_K$ varies and shrinks down following the specimen width *W*, as reported in Table 1. Alternatively, results of Figure 5 can also be plotted against the singular stress field length obtained from MS analyses $\Lambda_{K\text{-}MS}$. However, since the author wanted to underline the breakdown of the continuum formulation, $\Lambda_K$ was employed. Additionally, Table 1 reports the values of $\Lambda_{K\text{-}MS}$ and intriguingly shows that the $\Lambda_{K\text{-}MS}$ is on average always larger than $\Lambda_K$. However, as mentioned earlier, a direct comparison between stress fields should be carried out cautiously, and the values are reported for the sake of completeness only.

## 4. Conclusion

The present work presented a series of virial stress-based molecular statistics (MS) analyses on single-edge cracked samples made of ideal brittle silicon, while scaling down the sample until few nanometers. The virial stress was used as a measure of the mechanical stress at the atomic level, and stress intensity factor at failure is evaluated according to Irwin's definition. Subsequently, a series of continuum-based FE analyses were realized based on the failure conditions obtained from the MS analyses. Provided that the virial stress is accepted as a measure of the stress at the atomic level, the main findings can be summarized as follows

- As the specimen width is reduced, the atomistic stress field shrinks down but still varies with $1/r^{0.5}$, according to classic formulation; and a stress intensity factor at failure can be derived for all the geometries based on the virial stress.
- The stress intensity factor at failure from virial stress is constant and in perfect agreement with values available in the literature for nanosamples, microsamples, and bulk material.
- It is demonstrated again that the fracture toughness in the case of ideal brittle fracture in silico is scale-independent.
- Linear elastic fracture mechanics applied to the atomic stress field is still able to characterize the crack-tip region, at least for ideal brittle fracture and static crack.
- Continuum values, obtained from FE analyses, show a constant stress intensity factor at failure only for large specimens and fail to describe the fracture below a critical size of $W \approx 50$ nm.
- The breakdown of continuum-based fracture mechanics in the case of ideal brittle fracture is explained based on the singular stress field length and fracture process zone: when the ratio $\Lambda_K/R_{FPZ}$ is about 4–5 (i.e., $\Lambda_K = 1.6$ to 2 nm), continuum formulation does not hold and gives an apparent size-dependent (decreasing) stress intensity factor at fracture (failure conditions).

The present work demonstrated that the concept of stress intensity factor is still surprisingly valid if the atoms are modeled, and thus shows that values from atomic stress may be useful to describe the fracture criterion at extremely small dimensions. As a future step, it would be interesting to realize a direct comparison of the stress fields, investigate their equivalence, and to employ two-parameters models to consider non-singular terms in the continuum formulation.

## 5. Experimental Section

*Molecular Statistics (MS) Simulations*: The fracture tests are conducted by using the open-source code LAMMPS.[46] The modified Stillinger–Weber (SW) interatomic potential[13,14,35] is employed in the simulations, that is, ideal brittle fracture in silico is considered. The potential provides a good description of the stress concentration phenomena,[36,40] and it is therefore employed in the present study. The samples have the face-centered diamond-cubic structure of single-crystal silicon and are oriented as depicted in Figure 1a. The crack plane coincides with the cleavage plane (111), and it is perpendicular to the direction [111]. The elasticity tensor for a cubic crystal symmetry has three independent constants and assumes the following form in the crystal frame:[47,48]

$$\begin{pmatrix} C_{11} & C_{12} & C_{12} & 0 & 0 & 0 \\ C_{12} & C_{11} & C_{12} & 0 & 0 & 0 \\ C_{12} & C_{12} & C_{11} & 0 & 0 & 0 \\ 0 & 0 & 0 & C_{44} & 0 & 0 \\ 0 & 0 & 0 & 0 & C_{44} & 0 \\ 0 & 0 & 0 & 0 & 0 & C_{44} \end{pmatrix}.$$

Note that the elasticity tensor has to be rotated from the *crystal frame* to the *sample orientation* before to be employed in FE simulations. The SW potential gives the following properties: material constants $C_{11}$, $C_{12}$, and $C_{44}$ of 201 GPa, 51.4 GPa and 90.5 GPa, respectively; a lattice constant of

5.431 Å; ideal material strength $\sigma_{IS}$ of 35.2 GPa at a critical strain $\varepsilon_C$ of 0.3 along the direction [111]. The ideal material strength is the maximum ideal strength of a component ideally defect-free, and it has been evaluated from the un-cracked sample.[21]

A stepwise increment of strain $\varepsilon$ is applied at the upper and lower layers of atoms of the specimens, as shown in Figure 1. The strain is increased at each load-step until the maximum displacement before final fracture $d_C$ is reached. Periodic boundary conditions are applied along the *z*-direction while the simulation box has a finite thickness *t* in the *z*-direction of ≈0.384 nm. At the beginning of each strain/load increment, relaxation is ensured by using the damped dynamics method Fast Inertial Relaxation Engine (FIRE)[49] until all forces on atoms become less than $1.0 \times 10^{-5}$ $\mu$N. The traction-free crack is realized by deleting interactions between atoms along the pre-crack surfaces artificially. Note: the atomic stress computed by LAMMPS is a stress × volume formulation, meaning the computed quantity is in units of pressure × volume. It would need to be divided by a per-atom volume to have units of stress (pressure). In the present work, the per-atom volume is calculated using the unit cell volume at the critical strain $\varepsilon_C = 0.3$ rather than the volume given by the lattice constant. The single crystal silicon has a diamond cubic structure with eight atoms in a single unit cell, which gives a per-atom volume of 24.55 Å$^3$ (at the critical strain). See Section 2 for additional comments and justifications. Analyses are conducted at a temperature of 0 K and fully including the lattice trapping,[50,51] as commented in Section 2.

*Finite-Element (FE) Analyses*: Samples were modeled by using the *Ansys APDL 15.0* finite element software package. A 2D eight-node element-type PLANE183 and plane strain condition were assumed. Elements close to the crack-tip were approximately smaller than $a/10^6$ (where *a* is the crack length). The linear elastic anisotropic material model was used. Note that the elasticity tensor provided before has to be rotated from the *crystal frame* to the *sample orientation* of Figure 1 before to be employed in the FE simulations. Moreover, *Ansys APDL 15.0* expects the order of vector as {*x*, *y*, *z*, *xy*, *yz*, *xz*}, whereas for some published materials the order is given as {*x*, *y*, *z*, *yz*, *xz*, *xy*}. Therefore, the stiffness matrix has to be first rotated and later converted to the expected format.

The constraints configuration of the model is shown in Figure 1b. Displacement at critical load before final fracture $d_C$, obtained from MS simulations, was applied for each geometry. Thus, the continuum FE analyses are based on the failure conditions obtained from MS analyses.

## Acknowledgements

The work was partially carried out at Kyoto University, during the Japan Society for the Promotion of Science (JSPS) fellowship (Grant Number: 16F16366). The author is grateful to Prof. T. Sumigawa, Prof. T. Kitamura, and particularly to Prof. T. Shimada (Kyoto University) for his support during the development of the present work.

## Conflict of Interest

The author declares no conflict of interest.

## Keywords

atomistic simulations, brittle, crack, fracture, silicon, singularity, virial stress

Received: July 30, 2019
Revised: August 9, 2019
Published online:

[1] D. Akinwande, N. Petrone, J. Hone, *Nat. Commun.* **2014**, *5*, 5678.
[2] H.-Y. Chang, M. N. Yogeesh, R. Ghosh, A. Rai, A. Sanne, S. Yang, N. Lu, S. K. Banerjee, D. Akinwande, *Adv. Mater.* **2016**, *28*, 1818.
[3] T. Shimada, T. Kitamura, in *Advanced Structured Materials* (Eds: H. Altenbach, T. Matsuda, D. Okumura), Springer International Publishing, Cham, Switzerland **2015**, pp. 379–396.
[4] T. Sumigawa, H. Fang, E. Kawai, T. Kitamura, *Mech. Eng. Rev.* **2014**, *1*, SMM0007.
[5] T. Sumigawa, K. Byungwoon, Y. Mizuno, T. Morimura, T. Kitamura, *Acta Mater.* **2018**, *153*, 270.
[6] K. F. Wang, B. L. Wang, T. Kitamura, *Acta Mech. Sin.* **2016**, *32*, 83.
[7] P. Gallo, T. Sumigawa, T. Shimada, Y. Yan, T. Kitamura, in *Proceedings of the First International Conference on Theoretical, Applied and Experimental Mechanics* (Ed: E. E. Gdoutos), Springer International Publishing, Cham, Switzerland **2019**, pp. 205–210.
[8] P. Gallo, T. Sumigawa, T. Kitamura, *Frattura Integr. Strutt.* **2019**, *13*, 408.
[9] P. Gallo, T. Sumigawa, T. Kitamura, F. Berto, *Theor. Appl. Fract. Mech.* **2018**, *95*, 261.
[10] P. Gallo, Y. Yan, T. Sumigawa, T. Kitamura, *Adv. Theory Simul.* **2018**, *1*, 1700006.
[11] W. Zhang, J. Hu, J. Tang, Z. Wang, J. Wang, T. Lu, Z. Suo, *ACS Macro Lett.* **2019**, *8*, 17.
[12] C. Lamuta, A. Cupolillo, A. Politano, Z. S. Aliev, M. B. Babanly, E. V. Chulkov, L. Pagnotta, *Nano Res.* **2016**, *9*, 1032.
[13] D. Holland, M. Marder, *Adv. Mater.* **1999**, *11*, 793.
[14] D. Holland, M. Marder, *Phys. Rev. Lett.* **1998**, *80*, 746.
[15] N. M. Pugno, R. S. Ruoff, *Philos. Mag.* **2004**, *84*, 2829.
[16] N. Pugno, A. Carpinteri, M. Ippolito, A. Mattoni, L. Colombo, *Eng. Fract. Mech.* **2008**, *75*, 1794.
[17] A. A. Griffith, *Philos. Trans. R. Soc., A* **1921**, *221*, 163.
[18] T. Shimada, K. Ouchi, Y. Chihara, T. Kitamura, *Sci. Rep.* **2015**, *5*, 8596.
[19] K. Huang, T. Shimada, N. Ozaki, Y. Hagiwara, T. Sumigawa, L. Guo, T. Kitamura, *Int. J. Solids Struct.* **2017**, *128*, 67.
[20] T. Sumigawa, T. Shimada, S. Tanaka, H. Unno, N. Ozaki, S. Ashida, T. Kitamura, *ACS Nano* **2017**, *11*, 6271.
[21] P. Gallo, Y. Hagiwara, T. Shimada, T. Kitamura, *Theor. Appl. Fract. Mech.* **2019**, *103*, 102300.
[22] A. Needleman, E. Van der Giessen, *MRS Bull.* **2001**, *26*, 211.
[23] B. Shiari, R. E. Miller, *J. Mech. Phys. Solids* **2016**, *88*, 35.
[24] E. B. Tadmor, R. Phillips, M. Ortiz, *Langmuir* **1996**, *12*, 4529.
[25] A. K. Nair, D. H. Warner, R. G. Hennig, W. A. Curtin, *Scr. Mater.* **2010**, *63*, 1212.
[26] J. J. Möller, E. Bitzek, R. Janisch, H. ul Hassan, A. Hartmaier, *J. Mater. Res.* **2018**, *33*, 3750.
[27] G. R. Irwin, *J. Appl. Mech.* **1957**, *24*, 361.
[28] H. M. Westergaard, *J. Appl. Mech.* **1939**, *61*, A49.
[29] S. H. Cheng, C. T. Sun, *Int. J. Solids Struct.* **2014**, *51*, 2027.
[30] A. K. Subramaniyan, C. T. Sun, *Int. J. Solids Struct.* **2008**, *45*, 4340.
[31] J.-L. Tsai, S.-H. Tzeng, Y.-J. Tzou, *Int. J. Solids Struct.* **2010**, *47*, 503.
[32] S. Xu, X. Deng, *Nanotechnology* **2008**, *19*, 115705.
[33] A. Mattoni, L. Colombo, F. Cleri, *Phys. Rev. B* **2004**, *70*, 094108.
[34] M. Zhou, *Proc. R. Soc. London, Ser. A* **2003**, *459*, 2347.
[35] F. H. Sillinger, T. A. Weber, *Phys. Rev. B* **1985**, *31*, 5262.
[36] J. R. Kermode, T. Albaret, D. Sherman, N. Bernstein, P. Gumbsch, M. C. Payne, G. Csányi, A. De Vita, *Nature* **2008**, *455*, 1224.
[37] J. A. Zimmerman, E. B. WebbIII, J. J. Hoyt, R. E. Jones, P. A. Klein, D. J. Bammann, *Modell. Simul. Mater. Sci. Eng.* **2004**, *12*, S319.
[38] P. S. Branicio, D. J. Srolovitz, *J. Comput. Phys.* **2009**, *228*, 8467.
[39] N. C. Admal, E. B. Tadmor, *J. Elasticity* **2010**, *100*, 63.
[40] G. Singh, J. R. Kermode, A. De Vita, R. W. Zimmerman, *Int. J. Fract.* **2014**, *189*, 103.

 

[41] T. Sumigawa, S. Ashida, S. Tanaka, K. Sanada, T. Kitamura, *Eng. Fract. Mech.* **2015**, *150*, 161.
[42] J. R. Kermode, A. Gleizer, G. Kovel, L. Pastewka, G. Csányi, D. Sherman, A. De Vita, *Phys. Rev. Lett.* **2015**, *115*, 1.
[43] S.-H. Cheng, C. T. Sun, *J. Nanomech. Micromech.* **2014**, *4*, A4014001.
[44] A. H. Sherry, C. C. France, M. R. Goldthorpe, *Fatigue Fract. Eng. Mater. Struct.* **1995**, *18*, 141.
[45] G. H. Lee, Y. J. Chung, S. M. Na, H. G. Beom, *J. Mech. Sci. Technol.* **2018**, *32*, 3765.
[46] S. Plimpton, *J. Comput. Phys.* **1995**, *117*, 1.
[47] M. A. Hopcroft, W. D. Nix, T. W. Kenny, *J. Microelectromech. Syst.* **2010**, *19*, 229.
[48] J. J. Wortman, R. A. Evans, *J. Appl. Phys.* **1965**, *36*, 153.
[49] E. Bitzek, P. Koskinen, F. Gähler, M. Moseler, P. Gumbsch, *Phys. Rev. Lett.* **2006**, *97*, 170201.
[50] R. Thomson, C. Hsieh, V. Rana, *J. Appl. Phys.* **1971**, *42*, 3154.
[51] N. Bernstein, D. W. Hess, *Phys. Rev. Lett.* **2003**, *91*, 1.
[52] A. Stukowski, *Modell. Simul. Mater. Sci. Eng.* **2010**, *18*, 015012.